Image formation properties and inverse imaging problem in aperture based scanning near field optical microscopy

S. Schmidt,[1,2,*] A. E. Klein,[2] T. Paul,[1] H. Gross,[1,2] S. Diziain,[2] M. Steinert,[2] A. C. Assafrao,[3] T. Pertsch,[2] H. P. Urbach,[3] and C. Rockstuhl[4,5]

[1] *Fraunhofer Institute of Applied Optics and Precision Engineering, 07745 Jena, Germany*
[2] *Friedrich-Schiller-Universität Jena, Institute of Applied Physics, Abbe Center of Photonics, 07743 Jena, Germany*
[3] *Optics Research Group, Department of Imaging Science and Technology, Delft University of Technology, 2628 CJ Delft, The Netherlands*
[4] *Institute of Theoretical Solid State Physics, Karlsruhe Institute of Technology, 76131 Karlsruhe, Germany*
[5] *Institute of Nanotechnology, Karlsruhe Institute of Technology, 76021 Karlsruhe, Germany*
[*] *soeren.schmidt@iof.fraunhofer.de*

Abstract: Aperture based scanning near field optical microscopes are important instruments to study light at the nanoscale and to understand the optical functionality of photonic nanostructures. In general, a detected image is affected by both the transverse electric and magnetic field components of light. The discrimination of the individual field components is challenging as these four field components are contained within two signals in the case of a polarization resolved measurement. Here, we develop a methodology to solve the inverse imaging problem and to retrieve the vectorial field components from polarization and phase resolved measurements. Our methodology relies on the discussion of the image formation process in aperture based scanning near field optical microscopes. On this basis, we are also able to explain how the relative contributions of the electric and magnetic field components within detected images depend on the chosen probe. We can therefore also describe the influence of geometrical and material parameters of individual probes within the image formation process. This allows probes to be designed that are primarily sensitive either to the electric or magnetic field components of light.

OCIS codes: (180.4243) Near-field microscopy; (350.4238) Nanophotonics and photonic crystals; (250.5403) Plasmonics; (050.6624) Subwavelength structures.

References and links

1. M. Schnell, A. Garcia-Etxarri, A. J. Huber, K. B. Crozier, A. Borisov, J. Aizpurua, and R. Hillenbrand, “Amplitude- and phase-resolved near-field mapping of infrared antenna modes by transmission-mode scattering-type near-field microscopy,” J. Phys. Chem. C **114**, 7341–7345 (2010).
2. M. Esslinger, J. Dorfmüller, W. Khunsin, R. Vogelgesang, and K. Kern, “Background-free imaging of plasmonic structures with cross-polarized apertureless scanning near-field optical microscopy,” Rev. Sci. Instrum. **83**, 033704 (2012).
3. R. Esteban, R. Vogelgesang, J. Dorfmüller, A. Dmitriev, C. Rockstuhl, C. Etrich, and K. Kern, “Direct near-field optical imaging of higher order plasmonic resonances,” Nano Lett. **8**, 3155–3159 (2008).

#256987 Received 6 Jan 2016; revised 7 Feb 2016; accepted 8 Feb 2016; published 19 Feb 2016

4. S. Diziain, D. Barchiesi, T. Grosges, and P.-M. Adam, "Recovering of the apertureless scanning near-field optical microscopy signal through a lock-in detection," Appl. Phys. B **84**, 233–238 (2006).
5. B. le Feber, N. Rotenberg, D. M. Beggs, and L. Kuipers, "Simultaneous measurement of nanoscale electric and magnetic optical fields," Nature Photon. **8**, 43–46 (2013).
6. B. le Feber, N. Rotenberg, D. van Oosten, and L. Kuipers, "Modal symmetries at the nanoscale: a route toward a complete vectorial near-field mapping," Opt. Lett. **39**, 2802–2805 (2014).
7. N. Rotenberg and L. Kuipers, "Mapping nanoscale light fields," Nature Photon. **8**, 919–926 (2014).
8. J. N. Walford, J. A. Porto, R. Carminati, and J.-J. Greffet, "Theory of near-field magneto-optical imaging," J. Opt. Soc. Am. A **19**, 572–583 (2002).
9. J. A. Porto, R. Carminati, and J.-J. Greffet, "Theory of electromagnetic field imaging and spectroscopy in scanning near-field optical microscopy," J. Appl. Phys. **88**, 4845 (2000).
10. D. K. Singh, J. S. Ahn, S. Koo, T. Kang, J. Kim, S. Lee, N. Park, and D.-S. Kim, "Selective electric and magnetic sensitivity of aperture probes," Opt. Express **23**, 20820–20828 (2015).
11. E. Devaux, A. Dereux, E. Bourillot, Y. Weeber, J. C. Lacroute, J. Goudonnet, and C. Girard, "Local detection of the optical magnetic field in the near zone of dielectric samples," Phys. Rev. B **62**, 10504 (2000).
12. A. Dereux, E. Devaux, J. C. Weeber, J. P. Goudonnet, and C. Girard, "Direct interpretation of near-field optical images," J. Microsc. **202**, 320–331 (2001).
13. A. E. Klein, N. Janunts, M. Steinert, A. Tünnermann, and T. Pertsch, "Polarization-resolved near-field mapping of plasmonic aperture emission by a dual-snom system," Nano Lett. **14**, 5010–5015 (2014). PMID: 25088302.
14. A. E. Klein, A. Minovich, M. Steinert, N. Janunts, A. Tünnermann, and T. Pertsch, "Controlling plasmonic hot spots by interfering airy beams," Opt. Lett. **37**, 3402–3404 (2012).
15. M. Burresi, D. van Oosten, T. Kampfrath, H. Schoenmaker, R. Heideman, A. Leinse, and L. Kuipers, "Probing the magnetic field of light at optical frequencies," Science **326**, 550–553 (2009).
16. A. Minovich, A. E. Klein, N. Janunts, and T. Pertsch, "Generation and near-field imaging of airy surface plasmons," Phys. Rev. Lett. **107**, 116802 (2011).
17. A. Bouhelier, F. Ignatovich, A. Bruyant, C. Huang, G. Colas des Francs, and J.-C. Weeber, "Surface plasmon interference excited by tightly focused laser beams," Opt. Lett. **32**, 2535–2537 (2007).
18. M. Burresi, A. Engelen, R. Opheij, D. van Oosten, D. Mori, T. Baba, and L. Kuipers, "Observation of polarization singularities at the nanoscale," Phys. Rev. Lett. **102**, 2480–2483 (2009).
19. M. Burresi, T. Kampfrath, D. van Oosten, J. C. Prangsma, B. S. Song, S. Noda, and L. Kuipers, "Magnetic light-matter interactions in a photonic crystal nanocavity," Phys. Rev. Lett. **105**, 123901 (2010).
20. P. Uebel, M. A. Schmidt, H. W. Lee, and P. S. Russell, "Polarisation-resolved near-field mapping of a coupled gold nanowire array," Opt. Express **20**, 28409–28417 (2012).
21. D. Denkova, N. Verellen, A. V. Silhanek, V. K. Valev, P. V. Dorpe, and V. V. Moshchalkov, "Mapping magnetic near-field distributions of plasmonic nanoantennas," ACS Nano **7**, 3168–3176 (2013).
22. D. Denkova, N. Verellen, A. V. Silhanek, P. Van Dorpe, and V. V. Moshchalkov, "Near-field aperture-probe as a magnetic dipole source and optical magnetic field detector," arXiv preprint arXiv:1406.7827 (2014).
23. D. C. Kohlgraf-Owens, S. Sukhov, and A. Dogariu, "Discrimination of field components in optical probe microscopy," Opt. Lett. **37**, 3606–3608 (2012).
24. H. W. Kihm, S. M. Koo, Q. H. Kim, K. Bao, J. E. Kihm, W. S. Bak, S. H. Eah, C. Lienau, H. Kim, P. Nordlander, N. Halas, N. Park, and D.-S. Kim, "Bethe-hole polarization analyser for the magnetic vector of light," Nat. Commun. **2**, 451 (2011).
25. H. W. Kihm, J. Kim, S. Koo, J. Ahn, K. Ahn, K. Lee, and N. Park, "Optical magnetic field mapping using a subwavelength aperture," Opt. Express **21**, 5625–5633 (2013).
26. R. M. Bakker, D. Permyakov, Y. F. Yu, D. Markovich, R. Paniagua-Domínguez, L. Gonzaga, A. Samusev, Y. Kivshar, B. Luk'yanchuk, and A. I. Kuznetsov, "Magnetic and electric hotspots with silicon nanodimers," Nano Lett. **15**, 2137–2142 (2015).
27. I. S. Sinev, P. M. Voroshilov, I. S. Mukhin, A. I. Denisyuk, M. E. Guzhva, A. K. Samusev, P. A. Belov, and C. R. Simovski, "Demonstration of unusual nanoantenna array modes through direct reconstruction of the near-field signal," Nanoscale **7**, 765–770 (2015).
28. C. Rockstuhl, T. Zentgraf, T. P. Meyrath, H. Giessen, and F. Lederer, "Resonances in complementary metamaterials and nanoapertures," Opt. Express **16**, 2080–2090 (2008).
29. F. J. Garcia de Abajo, "Colloquium: Light scattering by particle and hole arrays," Rev. Mod. Phys. **79**, 1267–1290 (2007).
30. A. Nesci, R. Dändliker, and H. P. Herzig, "Quantitative amplitude and phase measurement by use of a heterodyne scanning near-field optical microscope," Opt. Lett. **26**, 208–210 (2001).
31. M. Burresi, D. Diessel, D. van Oosten, S. Linden, M. Wegener, and L. Kuipers, "Negative-index metamaterials: Looking into the unit cell," Nano Lett. **10**, 2480–2483 (2010).
32. T. Grosjean, I. Ibrahim, M. Suarez, G. Burr, M. Mivelle, and D. Charraut, "Full vectorial imaging of electromagnetic light at subwavelength scale," Opt. express **18**, 5809–5824 (2010).
33. N. Caselli, F. La China, W. Bao, F. Riboli, A. Gerardino, L. Li, E. H. Linfield, F. Pagliano, A. Fiore, P. J. Schuck, S. Cabrini, A. Weber-Bargioni, M. Gurioli, and F. Intonti, "Deep-subwavelength imaging of both electric and

magnetic localized optical fields by plasmonic campanile nanoantenna," Sci. Rep. **5**, 9606 (2015).
34. J. J. Greffet and R. Carminati, "Image formation in near-field optics," Progr. Surf. Sci. **56**, 133–237 (1997).
35. D. Van Labeke and D. Barchiesi, "Probes for scanning tunneling optical microscopy: a theoretical comparison," J. Opt. Soc. Am. A **10**, 2193–2201 (1993).
36. B. Hecht, B. Sick, U. P. Wild, V. Deckert, R. Zenobi, O. J. F. Martin, and D. W. Pohl, "Scanning near-field optical microscopy with aperture probes: Fundamentals and applications," J. Chem. Phys **112**, 7761 (2000).
37. L. Novotny and C. Hafner, "Light propagation in a cylindrical waveguide with a complex, metallic, dielectric function," Phys. Rev. E **50**, 4094–4106 (1994).
38. L. Novotny and B. Hecht, *Principles of Nano-Optics* (Cambridge University, 2006).
39. A. W. Snyder and J. Love, *Optical Waveguide Theory* (Springer, 1983).
40. B. Dörband, H. Müller, and H. Gross, *Handbook of Optical Systems, Metrology of Optical Components and Systems* (Wiley-VCH, 2005) Vol. **5**.
41. W. Singer, M. Totzeck, and H. Gross, *Handbook of Optical Systems, Physical Image Formation* (Wiley-VCH, 2006) Vol. **2**.
42. M. Esslinger and R. Vogelgesang, "Reciprocity theory of apertureless scanning near-field optical microscopy with point-dipole probes," ACS Nano **6**, 8173–8182 (2012).
43. A. D. Rakic, A. B. Djurisic, J. M. Elazar, and M. L. Majewski, "Optical properties of metallic films for vertical-cavity optoelectronic devices," Appl. Opt. **37**, 5271–5283 (1998).
44. R. Dorn, S. Quabis, and G. Leuchs, "Sharper focus for a radially polarized light beam," Phys. Rev. Lett. **91**, 233901 (2003).
45. L. Novotny, M. Beversluis, K. Youngworth, and T. Brown, "Longitudinal field modes probed by single molecules," Phys. Rev. Lett. **86**, 5251 (2001).
46. L. Rabiner, R. Schafer, and C. Rader, "The chirp z-transform algorithm," IEEE Trans Sig. Process. **17**, 86–92 (1969).
47. S. Roose, B. Brichau, and E. Stijns, "An efficient interpolation algorithm for Fourier and diffractive optics," Opt. Commun. **97**, 312–318 (1992).
48. J. Bakx, "Efficient computation of optical disk readout by use of the chirp z transform," Appl. Opt. **41**, 4897–4903 (2002).
49. W. Smigaj, P. Lalanne, J. Yang, T. Paul, C. Rockstuhl, and F. Lederer, "Closed-form expression for the scattering coefficients at an interface between two periodic media," Appl. Phys. Lett. **98**, 111107 (2011).

1. Introduction

The optical near field is a key quantity in nano-optics, which is the domain of research that deals with the interaction of light with objects having a critical length scale in the order of a few up to hundreds of nanometers. Only in the near field does the fraction of the angular spectrum that is associated with evanescent waves have a notable amplitude. These evanescent field components carry the high spatial frequency information of the underlying electromagnetic field. Experimental access to the near fields, therefore, is often important for understanding the interplay between photonic nanostructures and an incident light field. This triggered the development of scanning near field optical microscopes (SNOMs). These instruments rely on the perturbation of the near field by a sharp tip. In this scattering process, roughly spoken, evanescent waves are converted to propagating waves that can be detected by classical instruments in the far field. This basic idea led to different instrumental implementations.

In an apertureless (also called scattering) SNOM, a tip with an apex size of several nanometers scatters the light from the near into the far field [1–4]. Alternatively, more compact devices based on an aperture version of the SNOM were developed. There, a tapered waveguide is covered with a metallic film. A small opening at the apex locally collects the light. For such aperture SNOMs, which we study in this investigation, it was predicted and proven that detected signals are influenced by both the transverse electric and magnetic components of the investigated field [5–10]. Depending on the measurement configuration, a detected signal can be influenced dominantly by either the transverse electric, magnetic, or both field components [5–7, 10–27]. Nevertheless, analytical expressions that allow the evaluation of the sensitivity of a probe to the individual investigated field components is missing.

Here, we derive semi-analytical expressions to describe the image formation process, which allows to identify and to evaluate the individual electric and magnetic components of the investigated field within a measurement. The expressions allow one to predict the influence of individual structural probe parameters within the image formation process. We discuss the properties that lead to the predominant detection of either the electric or the magnetic field components. We find that the geometry and the material composition of the probe at the measurement wavelength strongly affect which field component is measured. These detection characteristics are linked to plasmonic resonances in the aperture of the probe, which are strongly influenced by geometrical and material parameters [28, 29]. These insights provide indications for aperture SNOM probes that predominantly measure the electric or the magnetic field components. Alternatively to experimental studies in which the influence of the aperture size and the metal coating thickness were investigated [5, 10], we investigate the influence of the coating material. Specifically, we study a probe coated by either gold, which can be predominantly sensitive to the magnetic components, or aluminum, which can be predominantly sensitive to the electric components of an investigated field at a specific spectral region.

In a further step, we discuss the solution of the inverse imaging problem without prior assumptions concerning the collection efficiency of probes or underlying field symmetries. This can create unprecedented metrological opportunities to characterize electromagnetic fields at the nanoscale. By relying on a polarization and phase resolved measurement, being available with the current state-of-the-art technology [5, 6, 15, 18, 19, 30, 31], two distinct signals are gathered. These two signals correspond to the complex amplitudes of two orthogonally polarized modes of the fiber that transmits the signal to the far field. These two complex signals, in general, are influenced by four complex quantities, namely the transverse in-plane electric and magnetic components of the investigated field. The coupling of these field components, through the collection of the signals by the probe and their simultaneous contribution to the two measurement signals, makes it challenging to directly compare measured images in the two signals with any of the components of the field which are to be measured.

It was already proven, that with suitable *a priori* knowledge, the coupling can be resolved and the information about the investigated field components in a detected image can be decrypted [5–7, 32, 33]. This *a priori* knowledge contains information regarding the structural symmetries, the collection properties of the probe, or knowledge about the investigated field components. The decoupling without *a priori* knowledge is much more challenging. Nonetheless, the necessity of such image reconstruction was recently mentioned in a review as an important open issue [7]. To solve this issue, we provide here a methodology to resolve the coupling and thereby provide the ability to reconstruct the entire vectorial electromagnetic field information from polarization and phase resolved measurements without any prior knowledge.

Our results reside on the theoretical discussion of the image formation process in aperture based scanning near field optical microscopy. In particular, we discuss the coupling process of the field components to be detected with the eigenmodes sustained by the aperture of the SNOM-tip. The SNOM-tip is treated as a metal coated fiber. Hence, this approach is in close analogy to coupling problems studied in the context of classical fiber optics and provides a slightly alternative description when compared to the pioneering works presented in the past [8, 9, 34–36]. Our approach can be viewed as a special case of the general description provided within the early theories, while assuming a passive probe. In particular we assume that the probe does not influence the fields being measured. This was mentioned in [7], Rotenberg and Kuipers, to be mostly valid in practical situations. The advantage of our treatment relies on the simple interpretation of measured quantities. This permits us to identify the eigenmodes supported by the aperture as the coherent vectorial point-spread-functions of the aperture SNOM. Analysing these eigenmodes provides insights into the image formation process. We stress that the properties of the eigenmodes, depending on the geometry and the material composition of the tip, will have a strong impact on the image formation process. In particular, probes can

#256987 Received 6 Jan 2016; revised 7 Feb 2016; accepted 8 Feb 2016; published 19 Feb 2016

be engineered to be sensitive to either the transverse electric or magnetic components of the investigated field.

The paper is divided into two parts. In Sec. 2 the image formation and especially the conditions leading to the predominant detection of either the electric or the magnetic field components will be discussed. In Sec. 3 we focus on polarization and phase resolved measurements obtained by a heterodyne detection scheme and discuss the methodology to solve the inverse imaging problem. We provide an algorithmic approach to retrieve the four in-plane electromagnetic field components from the two polarization and phase resolved signals being measured.

2. Properties of the image formation process

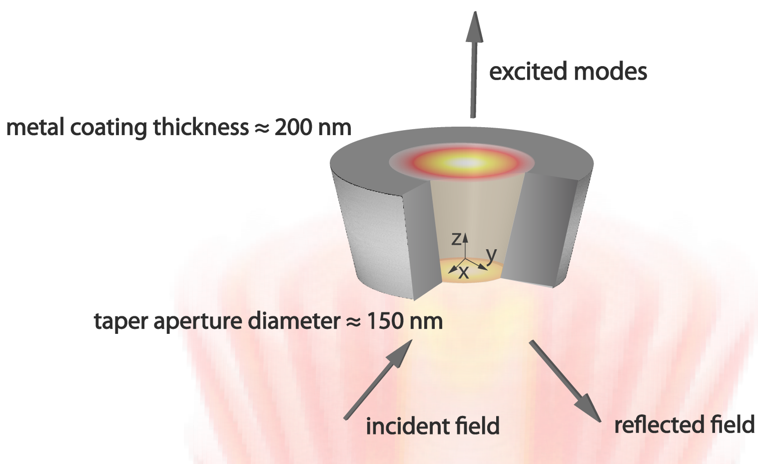

Fig. 1. Sketch of a typical probe used for aperture SNOM measurements in the visible wavelength range. The investigated field incident on the probe excites the modes supported by the aperture. The aperture should be understood as a metal coated fiber with the dimensions of the apex of the tip. The complete coupling process of the externally investigated field into the probe takes place only via the aperture, since the 200 nm thick metal coating prohibits any side coupling of light into the probe.

Understanding the coupling process of the investigated field, which carries structural information about the sample, into propagative modes in the fiber taper is at the heart of image formation in an aperture SNOM. The corresponding probe consists of a tapered dielectric optical fiber surrounded by a metal coating. In order to avoid any side coupling of light into the probe, the thickness of the metal coating is much larger than the skin depth at the wavelengths of interest. A subwavelength aperture is milled at the end of this taper (see Fig. 1). Due to the thick metal coating the coupling process of the investigated field into the tapered fiber occurs only via the aperture at the end of the taper. This suggests that the aperture itself can be understood as the converter for fields from the near into the far field that are guided by a fiber to the detector. To model the coupling process between the investigated field and the aperture at the apex of the SNOM tip, we treat the aperture as a cylindrical waveguide and calculate its eigenmodes. The excitation process of these modes by the external field, which is to be investigated, reveals all crucial information about the detected images. The derivation of the mathematical description of this excitation process is presented within Appendix A. Model. and is in close analogy to the early and pioneering works [8, 9, 34–36].

#256987 Received 6 Jan 2016; revised 7 Feb 2016; accepted 8 Feb 2016; published 19 Feb 2016

Due to the deep subwavelength size of the aperture, it supports only two propagative modes. They are indicated in the following by the subscript 1 and 2. With z as the principal propagation direction, these are the mainly x- and y-polarized states of the generalized HE_{11} - modes in the aperture (see Fig. 2) [37, 38]. The electric field of the two modes is given by $\mathbf{e}_{1,2}(x,y)$. The magnetic field of the two modes is given by $\mathbf{h}_{1,2}(x,y)$. A further superscript $+$ denotes forward propagating modes. A further superscript $-$ denotes backward propagating modes. The excitation coefficients t_1, t_2 of the forward propagating fundamental x- and y- polarized modes excited by an external field can be calculated (see Appendix A. Model. for details) as

$$\begin{aligned} t_1(x,y) &= \int_{\mathscr{R}^2} [\mathbf{e}_1^-(\tilde{x}-x,\tilde{y}-y)\times\mathbf{H}(\tilde{x},\tilde{y})-\mathbf{E}(\tilde{x},\tilde{y})\times\mathbf{h}_1^-(\tilde{x}-x,\tilde{y}-y)]\,\mathbf{n}_z\,d\tilde{x}\,d\tilde{y}, \quad (1)\\ t_2(x,y) &= \int_{\mathscr{R}^2} [\mathbf{e}_2^-(\tilde{x}-x,\tilde{y}-y)\times\mathbf{H}(\tilde{x},\tilde{y})-\mathbf{E}(\tilde{x},\tilde{y})\times\mathbf{h}_2^-(\tilde{x}-x,\tilde{y}-y)]\,\mathbf{n}_z\,d\tilde{x}\,d\tilde{y}\,. \end{aligned}$$

According to the unconjugated reciprocity theorem, the mode coefficients of the forward $+$ propagating modes are calculated by projecting the investigated field onto the backward propagating $-$ ones. $\mathbf{E}(\tilde{x},\tilde{y})$ and $\mathbf{H}(\tilde{x},\tilde{y})$ in these equation correspond to the time harmonic electromagnetic field components of the investigated field in the plane $z=0$. This plane is defined by the height of the aperture and $(x,y)^T$ defines the position of the tip (see Fig. 1). The time resolved harmonic fields depending on the frequency ω are given by $\mathscr{E}(x,y,z=0,t)=\mathbf{E}(x,y)\,e^{-i\omega t}$ and $\mathscr{H}(x,y,z=0,t)=\mathbf{H}(x,y)\,e^{-i\omega t}$. The image that is detected corresponds to the guided power of the modes supported by the aperture [39]

$$\begin{aligned} \mathscr{I}(x,y) = {} & |t_1(x,y)|^2+|t_2(x,y)|^2 \\ = {} & \left|\int_{\mathscr{R}^2} [\mathbf{e}_1^-(\tilde{x}-x,\tilde{y}-y)\times\mathbf{H}(\tilde{x},\tilde{y})-\mathbf{E}(\tilde{x},\tilde{y})\times\mathbf{h}_1^-(\tilde{x}-x,\tilde{y}-y)]\,\mathbf{n}_z\,d\tilde{x}\,d\tilde{y}\right|^2 + \quad (2)\\ & \left|\int_{\mathscr{R}^2} [\mathbf{e}_2^-(\tilde{x}-x,\tilde{y}-y)\times\mathbf{H}(\tilde{x},\tilde{y})-\mathbf{E}(\tilde{x},\tilde{y})\times\mathbf{h}_2^-(\tilde{x}-x,\tilde{y}-y)]\,\mathbf{n}_z\,d\tilde{x}\,d\tilde{y}\right|^2. \end{aligned}$$

The above formulation allows one to interpret the eigenmodes sustained by the aperture as the coherent point-spread-function of the aperture SNOM. Then the result can be regarded in terms of classical microscopy under coherent illumination, where the image is correspondingly formed as the convolution between the coherent point-spread-function and the field of the investigated structure of interest in the case of an isoplanatic condition [40, 41]. However, in contrast to classical microscopy, the point spread function in aperture based SNOM is vectorial, encoding not only electric but also magnetic field components in a detected image. From the expression above it becomes evident that the dominance of either the electric or the magnetic field components in a detected image not only depends on the investigated field but also on the electromagnetic properties of the two modes accessible in the aperture.

The further distinction of individual field components contributing to a detected image in Eq. (2) is impossible, in general, due to the encryption through the convolution process. To gain a deeper insight into the relation between investigated field components and a detected image, we make the assumption from now on that the fields being measured are constant across the spatial extent of the modes sustained by the aperture. In lowest order approximation this corresponds to the assumption that the fields are constant across the spatial extent of the aperture. This assumption can be enforced by either using sufficiently small apertures or by measuring the fields at a certain distance relative to the subject, i.e. at a distance where rapidly oscillating spatial field components have decayed. The advantage of this approximation is the ability to derive semi-analytical expressions for the measured intensity. They enable the identification of the measured field components in a detected image. This treatment departs from the

#256987 Received 6 Jan 2016; revised 7 Feb 2016; accepted 8 Feb 2016; published 19 Feb 2016

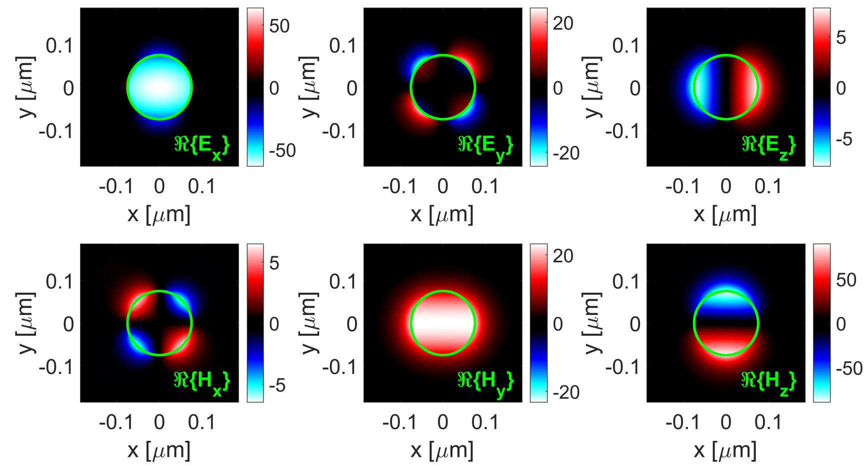

Fig. 2. Real part of the mainly x-polarized mode accessible in an aperture at a wavelength of 663 nm. The magnetic field components were multiplied by the free-space impedance $|Z_0|$, for better comparability of the field magnitudes. The aperture is made of fused-silica glass with a refractive index of $n = 1.5$ surrounded by a 200 nm thick gold coating. The e_x and h_y fields have a mirror-symmetry with respect to both coordinate axes x and y, whereas the e_y and h_x fields have an odd symmetry. The second accessible mode in the aperture is the mainly y-polarized one, in which the symmetries are reversed compared to the mainly x-polarized mode.

discussion of the image formation process in aperture SNOMs from its super-resolving character. Nevertheless, these assumptions have a considerable practical impact, as aperture SNOMs are often used to study non-propagating field components, i.e. related to plasmonic structures, where super-resolution is not necessarily required. In these cases, fundamental insights were often gathered while comparing measured images with simulated field distributions of the investigated structure [5–7, 11–15, 15–25]. The ability to directly relate measured images with simulated field components led to exceptional results, but is, in a strict sense, only possible when the aforementioned assumption is valid.

In the following the investigated field components are assumed to be constant across the aperture. Therefore, the fields, according to Eq. (2), are approximated by $\mathbf{E}(\tilde{x},\tilde{y}) = \mathbf{E}(x,y)$ and $\mathbf{H}(\tilde{x},\tilde{y}) = \mathbf{H}(x,y)$. Then the excitation strength corresponding to the mainly x-polarized mode within the aperture is given by

$$\begin{aligned} t_1(x,y) &= \int [\mathbf{e}_1^- \times \mathbf{H} - \mathbf{E} \times \mathbf{h}_1^-]\, \mathbf{n}_z \, d\tilde{x}\, d\tilde{y}\ , \\ &= H_y \int e_{1_x}^- d\tilde{x} d\tilde{y} - H_x \underbrace{\int e_{1_y}^- d\tilde{x} d\tilde{y}}_{=0} - E_x \int h_{1_y}^- d\tilde{x} d\tilde{y} + E_y \underbrace{\int h_{1_x}^- d\tilde{x} d\tilde{y}}_{=0}\ , \qquad (3) \\ &= H_y \underbrace{\int e_{1_x}^- \, d\tilde{x}\, d\tilde{y}}_{\overline{e_{1_x}}} - E_x \underbrace{\int h_{1_y}^- \, d\tilde{x}\, d\tilde{y}}_{\overline{h_{1_y}}}\ , \\ &= H_y \overline{e_{1_x}} - E_x \overline{h_{1_y}}\ . \qquad (4) \end{aligned}$$

Here the explicit dependencies on spatial coordinates were ommited to achieve a compact notation. In Eq. (3) two integrals vanish due to the odd symmetry of the corresponding mode

#256987 Received 6 Jan 2016; revised 7 Feb 2016; accepted 8 Feb 2016; published 19 Feb 2016

components (see Fig. 2). In the next step, the value $\overline{h_{1_y}}$ of the magnetic mode component of the mode in the aperture is expressed by the value $\overline{e_{1_x}}$ of the electric mode component of the aperture

$$\begin{aligned} \overline{h_{1_y}} &= {Z_M}^{-1}\,\overline{e_{1_x}}\ , \\ Z_M &= \frac{\overline{e_{1_x}}}{\overline{h_{1_y}}}\ . \end{aligned} \tag{5}$$

At this point, the mode impedance Z_M has been introduced. It expresses the ratio between the electric and magnetic mode components. By repeating the calculations for the mainly y-polarized mode accessible in the aperture, assuming a cylindrical symmetry of the probe, a final expression for the measured intensity can be derived that reads

$$\begin{aligned} \mathscr{I}(x,y) &= |t_1(x,y)|^2 + |t_2(x,y)|^2\ , \\ &= |\mathbf{H}_\perp(x,y)|^2 + |Z_M|^{-2}|\mathbf{E}_\perp(x,y)|^2 \\ &\quad -2|Z_M|^{-1}\,|E_x(x,y)|\,|H_y(x,y)|\cos(\phi_{Hy}(x,y)-\phi_{Ex}(x,y)-\phi_{Z_M}) \\ &\quad -2|Z_M|^{-1}\,|H_x(x,y)|\,|E_y(x,y)|\cos(\phi_{Hx}(x,y)-\phi_{Ey}(x,y)-\phi_{Z_M})\ . \end{aligned} \tag{6}$$

Here ϕ denotes the phase values of the complex quantities. Proportionality constants were neglected since they have no qualitative influence on the image formation. Here, cylindrical probe geometries were assumed with the tip placed perpendicular to the sample. For more general probe symmetries, the calculations have to be repeated, resulting in the possible fact that the mainly x-polarized mode is not coequal to the mainly y-polarized one. Moreover, probes that are inclined with respect to the sample require a modified version of Eq. (6). Then, the vectorial investigated field components need to be rotated into the coordinate frame defined by the tip.

The result obtained in Eq. (6) is one key finding of this work. The expression is applicable to directly explain a possible measurement and provides insights into the properties of the image formation process in aperture SNOMs. Specifically, two things become evident. On the one hand longitudinal field components, namely $|E_z|$ and $|H_z|$, cannot be detected. This is in agreement with past results [11, 12, 14–19, 21, 22, 24, 25]. Hence, the aperture SNOM is a complementary technique to the cross-polarized scattering-type SNOM, where $|E_z|$ is primarily measured [2, 3, 25, 42]. On the other hand, the mode impedance $|Z_M|$ influences the sensitivity of the aperture SNOM to detect either electric or magnetic field components. Therefore, it describes the impact of the probe itself on the measurement. This will be discussed in more detail in the following paragraph.

Equation 6 has two individual contributions which are called the amplitude and the phase terms in the following. Since these parts influence a detected image differently, their properties will be discussed individually. In the first step of the discussion, the phase term will be neglected.

The amplitude term, $|\mathbf{H}_\perp|^2 + |Z_M|^{-2}|\mathbf{E}_\perp|^2$, generally expresses the possibility to simultaneously measure the electric and magnetic field components. Their relative contributions are dictated by the impedance of the mode sustained by the aperture of the tip. To analyse the relative ratio of electric and magnetic field components contributing to a detected image, the ratio $\Gamma = \frac{|Z_M|^{-2}|\mathbf{E}_\perp|^2}{|\mathbf{H}_\perp|^2}$ is evaluated. By replacing $\frac{|\mathbf{E}_\perp|}{|\mathbf{H}_\perp|}$ with the transverse field impedance $|Z_\perp|$, the following result is obtained

$$\Gamma = \frac{|Z_\perp|^2}{|Z_M|^2}\quad . \tag{7}$$

#256987 Received 6 Jan 2016; revised 7 Feb 2016; accepted 8 Feb 2016; published 19 Feb 2016

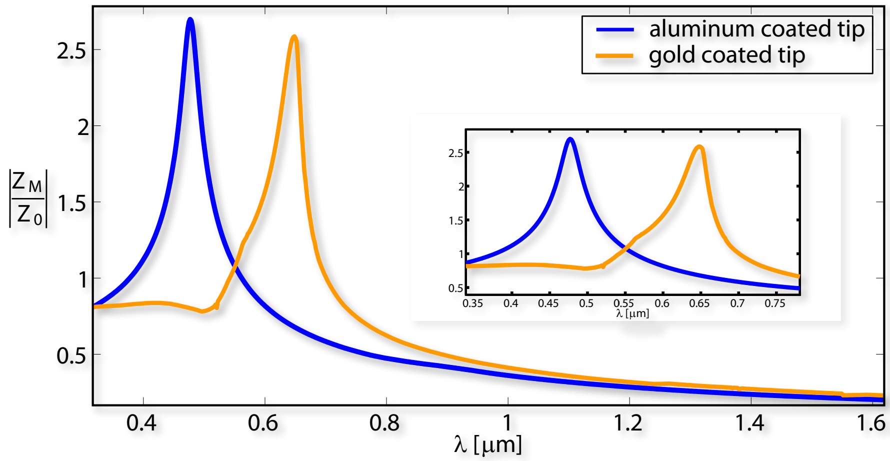

Fig. 3. Spectrally resolved mode-impedance factor $\left|\frac{Z_M(\lambda)}{Z_0}\right|$ for 2 commercially available probes normalized by the free-space impedance $Z_0 = 376\,\Omega$. Both tips share the same geometrical parameters, i.e. the aperture diameter is $D = 150$ nm, the core is made from fused silica with $n = 1.5$, and the core is covered with a 200 nm thick metal coating. The tips differ only by their coating material. Both probes show resonances of the mode-impedance in the visible wavelength range which are slightly shifted relative to each other. The resonance of the gold coated tip lies in the range of commonly used wavelengths for near field measurements with such aperture diameters. In this regime, around $\lambda = 650$ nm, gold coated probes tend to be much more sensitive to magnetic field components in a detected image when compared to aluminum coated tips.

It is the ratio between the investigated field and the mode impedance that determines the relative influence of the individual electric and magnetic field components in a detected image.

Since the mode impedance $|Z_M|$ depends on the geometry and the material of the tip, the detection properties of an aperture SNOM are strongly influenced by the choice of the probe. This is exemplified in Fig. 3, where the calculated spectrally resolved mode impedance $Z_M(\lambda)$ is shown for commercially available gold and aluminum coated probes with an aperture diameter D of $D = 150$ nm. All precise geometrical details of the tip are contained in the figure legend. Material properties as documented in literature have been considered [43]. The numerical analysis of the eigemodes guided in those apertures has been performed with COMSOL. It can be seen that both tips show strong resonances in the visible spectrum, leading to spectral variations in their detection characteristics. While the resonance for the gold coated probe lies at a wavelength of approximately $\lambda \approx 650$ nm, the resonance for the aluminum coated probe is shifted and lies at $\lambda \approx 470$ nm. These resonances originate from the excitation of localized surface plasmon polaritons in the aperture. This renders the tips not just sensitive on the aperture diameter but also to the material. Tailoring these resonances allows probes to be designed that are predominantly sensitive to either the electric or magnetic field components of light in a specific spectral region. By using Babinet's principle, the resonances of those apertures can be linked in lowest order approximation to resonances of cylindrical metallic nanoparticles, for which analytical means exist to predict the spectral position of the resonance [28, 29].

By assuming an electromagnetic field with the impedance of free space $Z_0 = 376\,\Omega$ to be investigated at a wavelength of $\lambda \approx 650$ nm, the image detected with the proposed gold coated tip would then, according to Eq. (7), be strongly influenced by magnetic field components.

#256987 Received 6 Jan 2016; revised 7 Feb 2016; accepted 8 Feb 2016; published 19 Feb 2016

It would be the opposite for the aluminum coated tip, in which the detected image would be dominated by electric field components.

Generally, for arbitrary electromagnetic fields, the investigated field impedance $|Z_{\perp}(x,y)|$ is a spatially varying quantity that depends on the local properties of the measured field. In a measurement, this behaviour causes a local variation of the predominant influence of either the electric or the magnetic field components in a detected image. These behaviours already have been investigated experimentally, in which the relative information content in a measurement related to electric and magnetic field parts was examined [5–7, 10]. There it was shown that the aperture size, the metal coating thickness, and the relative position on the sample changes the detection characteristics. Here, we can explain this experimental finding with Eq. (7) as the local variation of the impedances of the investigated field and the modes accessible in the aperture.

The ability to investigate electromagnetic fields with spatially distinguishable electric and magnetic field components, while strictly fulfilling the assumption that the field to be measured is constant across the aperture, is challenging. It requires the investigation of electromagnetic fields for which the intensity related to the time-averaged Poynting vector $<\mathbf{S}>= \frac{1}{2}\Re\{\mathbf{E}\times\mathbf{H}^*\}$ is not proportional to the local electric energy density $|\mathbf{E}|^2 \not\propto <\mathbf{S}>$. Possibilities for investigating electromagnetic fields with a strongly distinguishable character of the individual electric and magnetic components could be done by evaluating strongly focused radially polarized fields or alternatively standing wave patterns [44, 45].

Additionally, an unexpected influence on a measurement can be caused by a contribution of the phase term within the image formation process. Here, phase differences $\phi_{Hx}(x,y)-\phi_{Ey}(x,y)$ and $\phi_{Hy}(x,y)-\phi_{Ex}(x,y)$ between the local electric and magnetic field components influence a measurement. This effect can lead to unexpected influences on a detected image, making them difficult to interpret. To the best of our knowledge, emerging influences have not been reported in the literature. In case the investigated fields $\mathbf{E}$ and $\mathbf{H}$ additionally obey a slowly varying envelope approximation, the phase differences remain approximately constant across the scanning area. In these cases, the phase term then affects a detected image only by a decrease in contrast. This assumption, fully in line with the assumption that the field to be measured is constant across the aperture, might be satisfied with currently used aperture diameters of about $D_{\text{aperture}} \approx \frac{\lambda}{4}$.

3. Inverse imaging problem

In the previous section we discussed the image formation process in aperture SNOMs by assuming non-interferometric measurements, i.e. only the intensity of the modes have been considered. To expand on these results, we present in the following section an algorithm to reconstruct the complete vectorial electromagnetic field from a phase resolved measurement of the two excited eigenmodes. Such a measurement technique was developed during the last years, enabling the measurement of a polarization resolved signal in both amplitude and phase by using a heterodyne detection scheme [30]. The establishment of a heterodyne detection scheme for aperture based scanning near field measurements led to outstanding results [5–7, 15, 18, 19, 31].

Polarization and phase resolved signal

It is natural to assume that the polarization and phase resolved measured signals correspond to the excitation strengths of either the mainly x- or y-polarized mode $t_{1,2}(x,y)$ accessible in the aperture according to Eq. (1). In the analysis performed in the previous section it was shown that the recorded signals correspond either to a superposition of E_x and H_y or E_y and H_x (see Eq. (4)), which agrees with results presented by le Feber *et al.* in [5,6]. Correspondingly, within a measurement the four transverse electromagnetic field components are obtained within the

#256987 Received 6 Jan 2016; revised 7 Feb 2016; accepted 8 Feb 2016; published 19 Feb 2016

two polarization resolved signals. The discrimination of the individual field components in a detected image is challenging and requires a second set of equations or assumptions to resolve the discrepancy of an underdetermined system. This has already been shown by exploiting either an underlying symmetry, collection properties of the probe, or *a priori* knowledge of the investigated field components [5–7,32]. Here, we would like to discuss this issue in a more general way by solving the inverse imaging problem without prior knowledge about the structure or related symmetries. The principal approximation introduced to resolve the inverse imaging problem relies on the assumption of a passive probe that does not perturb the measured field, according to the model as presented in the Appendix A. Model. . This assumption was mentioned in [7], Rotenberg and Kuipers, to be mostly valid in practical situations. In the following analysis, the algorithmic approach to unravel the distinct field components will be presented.

We consider two conditions for the experimental setup. Once an eigenmode is excited at the apex, the amplitude of the mode is not influenced by any coupling process while it propagates through the fiber to a detector. Due to imperfections in an experimental setup, e.g. by fiber-bends, this might not be guaranteed. A coupling between the orthogonal modes due to imperfections might occur, causing a mixing of the individual detection paths. However, in reality, the problem can be experimentally solved by a prior calibration of the setup while investigating the transmission of linearly polarized light. By independently inspecting linearly x- and y-polarized fields, the Jones-Matrix of the SNOM can be determined. From the knowledge of these matrix entries in amplitude and phase, the polarization distortion introduced by weak disturbances within the measurement system can be analysed. It is then possible to remove the distortions numerically to infer the actual quantities of interest. Eventually, such calibration allows direct access to the complex, polarization resolved excitation coefficients according to Eq. (1). As a second assumption, we require the tip placed perpendicular to the sample. Otherwise, the investigated field components have to be rotated into the coordinate frame as defined by the orientation of the aperture of the tip. Then the following calculations that are outlined, have to be repeated with rotated field components. With these assumptions, we can continue to develop our field reconstruction algorithm.

Full vectorial field reconstruction

In this section, we present an algorithm to reconstruct the investigated field components from a phase resolved measurement. By introducing the Fourier-transformation for any of the quantities mentioned above (denoted here as $h(\mathbf{r}_\perp)$) that depend on the transverse coordinate $\mathbf{r}_\perp = (x,y)^\top$

$$\tilde{h}(\mathbf{k}_\perp) = \mathscr{F}\{h(\mathbf{r}_\perp)\} = \frac{1}{2\pi}\int_{\mathscr{R}^2} h(\mathbf{r}_\perp)\, e^{-i\left(k_x x + k_y y\right)} d\mathbf{r}_\perp$$

and its inverse

$$h(\mathbf{r}_\perp) = \mathscr{F}^{-1}\left\{\tilde{h}(\mathbf{k}_\perp)\right\} = \frac{1}{2\pi}\int_{\mathscr{R}^2} \tilde{h}(\mathbf{k}_\perp)\, e^{i\left(k_x x + k_y y\right)} d\mathbf{k}_\perp,$$

Eq. (1) can be written in Fourier domain as

$$\begin{aligned} \tilde{t}_1(\mathbf{k}_\perp) &= \left[\tilde{\mathbf{e}}_1^-(\mathbf{k}_\perp)\times\tilde{\mathbf{H}}(\mathbf{k}_\perp) - \tilde{\mathbf{E}}(\mathbf{k}_\perp)\times\tilde{\mathbf{h}}_1^-(\mathbf{k}_\perp)\right]\mathbf{n}_z, \\ \tilde{t}_2(\mathbf{k}_\perp) &= \left[\tilde{\mathbf{e}}_2^-(\mathbf{k}_\perp)\times\tilde{\mathbf{H}}(\mathbf{k}_\perp) - \tilde{\mathbf{E}}(\mathbf{k}_\perp)\times\tilde{\mathbf{h}}_2^-(\mathbf{k}_\perp)\right]\mathbf{n}_z. \end{aligned} \tag{8}$$

Here quantities $\tilde{h}(\mathbf{k}_\perp)$ are the Fourier-representations of the respective functions $h(\mathbf{r}_\perp)$ in real space. Equation 8 can be understood as an underdetermined system of equations, where it is intended to determine the 4 unknown investigated field components $\tilde{E}_x, \tilde{E}_y, \tilde{H}_x, \tilde{H}_y$ in the Fourier domain from the measured and Fourier transformed mode coefficients $\tilde{t}_{1,2}$. By exploiting free

#256987 Received 6 Jan 2016; revised 7 Feb 2016; accepted 8 Feb 2016; published 19 Feb 2016

space Maxwell's Equations in the angular frequency domain, this limitation can be overcome and the apparent magnetic field components $\tilde{H}_x$ and $\tilde{H}_y$ can be equivalently expressed by the electric field components $\tilde{E}_x$, $\tilde{E}_y$. This results in a well determined system of equations

$$\begin{aligned}
\tilde{t}_1 &= \underbrace{\left(\gamma_3\tilde{e}^-_{1_x} - \gamma_1\tilde{e}^-_{1_y} - \tilde{h}^-_{1_y}\right)}_{M_{11}}\tilde{E}_x + \underbrace{\left(\gamma_4\tilde{e}^-_{1_x} - \gamma_2\tilde{e}^-_{1_y} + \tilde{h}^-_{1_x}\right)}_{M_{12}}\tilde{E}_y, \\
\tilde{t}_2 &= \underbrace{\left(\gamma_3\tilde{e}^-_{2_x} - \gamma_1\tilde{e}^-_{2_y} - \tilde{h}^-_{2_y}\right)}_{M_{21}}\tilde{E}_x + \underbrace{\left(\gamma_4\tilde{e}^-_{2_x} - \gamma_2\tilde{e}^-_{2_y} + \tilde{h}^-_{2_x}\right)}_{M_{22}}\tilde{E}_y, \\
\gamma_1 &= -\frac{1}{k_0 Z_0}\frac{k_y k_x}{k_z}, \qquad \gamma_2 = -\frac{1}{k_0 Z_0}\left(\frac{k_y^2}{k_z} + k_z\right), \\
\gamma_3 &= \frac{1}{k_0 Z_0}\left(\frac{k_x^2}{k_z} + k_z\right), \qquad \gamma_4 = \frac{1}{k_0 Z_0}\frac{k_y k_x}{k_z}, \\
k_z &= \sqrt{\left(\frac{2\pi}{\lambda}\right)^2 - k_x^2 - k_y^2}\,.
\end{aligned} \tag{9}$$

The individual matrices $M_{ik}(\mathbf{k}_\perp)$ can be interpreted as the vectorial transfer function of the SNOM-tip. It determines not just the spatial resolution but also the achievable contrast. These quantities are determined by the two fundamental modes accessible in the aperture and the individual matrices can be hence explicitly calculated.

The system of Eqns. 9 can be inverted independently for every transverse wave vector component $\mathbf{k}_\perp$ resulting in the two independent field components $\tilde{E}_x(\mathbf{k}_\perp)$ and $\tilde{E}_y(\mathbf{k}_\perp)$ in Fourier-representation. With this information, the remaining four field components $\tilde{E}_z(\mathbf{k}_\perp)$, $\tilde{H}_x(\mathbf{k}_\perp)$, $\tilde{H}_y(\mathbf{k}_\perp)$ and $\tilde{H}_z(\mathbf{k}_\perp)$ can be derived using Maxwell's equations for the homogeneous free space. By inversely Fourier transforming the independent field components, the investigated field can be reconstructed. The achievable resolution in the reconstructed investigated field components is limited by the accessible spatial frequencies in the different $M_{ik}(\mathbf{k}_\perp)$ matrices.

This algorithm has the capability to fully reconstruct all vectorial components of the investigated field. This approach allows one to extract information obtained by an aperture SNOM measurement without *a priori* knowledge and can provide novel insights in nano-optical research activities due to the ability to determine the complete vectorial information from a measurement.

From the numerical point of view, the only problem concerns the different discretizations of the investigated field and the modes supported by the aperture. Due to the nanoscopic dimensions of the aperture and the macroscopic extension of the investigated fields, the numerical sampling is different and has to be unified to evaluate Eq. (9). Due to the usual extreme ratio of the two different scales, approaches such as zero padding can cause difficult memory issues and prevent the calculation of the investigated field components. To prevent this problem, chirp z-transformations can be used to unify the grids without causing memory problems [41,46–48].

4. Conclusion

In conclusion, we discussed the properties of the image formation and the inverse imaging problem in aperture-based scanning near field optical microscopy. In particular, we derived semi-analytical expressions to describe the image formation process. They eventually allow one to assess the properties of aperture SNOM probes that lead to a predominant sensitivity to either the electric or the magnetic components of the investigated field in a detected image. We found that these detection characteristics are strongly linked to the properties of the modes sustained by the aperture of the SNOM. These properties can be tailored by changing the geometry and material composition of the probe, which constitutes the means by which a probe can be designed that can detect specific field components on demand. In particular, we proposed a specific probe that is either coated by aluminum or gold that primarily measures either the electric or magnetic field components at a specific wavelength. In addition, we provided a methodology to solve the inverse imaging problem to extract the complete vectorial field information from polarization and phase resolved measurements.

A. Appendix A model

Here, we discuss in detail the coupling process of the investigated field components with the modes supported by the aperture of the probe.

Due to the deep subwavelength size of the aperture, it supports only two propagative modes. These are the mainly x- and mainly y-polarized states of the generalized HE_{11} - modes in the aperture (see Fig. 2) [37, 38]. To conclude from the knowledge of these excitation strengths of the aperture modes on an image that can be measured by a detector, the aperture and the complete measurement setup needs to be considered simultaneously. We require here that the excitation strengths of the aperture modes are not modified by any coupling process with any other mode at a later stage of propagation through the system. This requires adiabatic modifications to the geometry of the fiber, e.g. while being tapered or being bent. Then, the modal amplitudes at the position of the detector are linearly related to the ones in the aperture.

The total power guided by the fiber to the detector is proportional to the absolute square of the excitation strengths of the supported modes [39]. Generally, the power can be written as $P = \sum_{i=1}^{\infty} |t_{i\,\text{detector}}|^2$, assuming orthogonal and power-normalized modes. In this case solely two modes are excited which are linearly related to the ones in the aperture. It follows that the guided power at the position of the detector can be written as $P \propto |t_{1\,\text{aperture}}|^2 + |t_{2\,\text{aperture}}|^2$. Consequently, we identify a detected image $\mathscr{I}$ via the guided power at the position of the detector from the knowledge of the excitation strengths in the aperture as $\mathscr{I} = |t_{1\,\text{aperture}}|^2 + |t_{2\,\text{aperture}}|^2$.

These excitation strengths depend on the position of the probe relative to the sample. Consequently, a detected image, when the probe scans the sample at a constant height, should be written as

$$\mathscr{I}(x,y) = |t_1(x,y)|^2 + |t_2(x,y)|^2 \ . \tag{10}$$

Here the excitation strengths of the mainly linearly polarized modes in the aperture were renamed as $t_{1,2} := t_{1,2\,\text{aperture}}$. These amplitude coefficients correspond to the projection of the investigated field onto the modes supported by the aperture. It follows that the detected image does not correspond to the investigated field components directly, but rather to the projection.

Keeping in mind the assumptions that were made, this approach simplifies the complex problem of the image formation process in aperture SNOMs to the question of understanding the coupling process of the two fundamental modes accessible in the aperture excited by the externally investigated field. This remaining problem can be regarded in terms of classical fiber optics and is in direct analogy to the treatment of splicing and coupling losses in optical fibers.

The incident field will couple power into the two propagative modes in the aperture, but also into the unbound radiation and the evanescent modes supported by the aperture. Additionally, it also causes a partial reflection of the incident field. To extract the coupling coefficients of the system, Maxwell's interface problem has to be solved at the position of the aperture. However, only the excitation coefficients for the guided modes are important. They will be derived in the following. In this derivation we assume monochromatic fields with a time dependence proportional to $e^{-i\omega t}$.

By formally introducing Dirac's notation, the transverse electromagnetic field of the m^{th} forward-propagating eigenmode in the aperture is denoted as $|\mathbf{T}_m^+\rangle$, where $m = 1, 2$ corresponds

#256987 Received 6 Jan 2016; revised 7 Feb 2016; accepted 8 Feb 2016; published 19 Feb 2016

to the mainly x- and mainly y-polarized mode of interest and any higher m stands for evanescent and radiation modes. The Dirac notation should be understood in the sense of a 4-component vector denoting the transverse mode profile as $|\mathbf{M}_m^+\rangle = [e_{x_m}(x,y), e_{y_m}(x,y), h_{x_m}(x,y), h_{y_m}(x,y)]^\top$, that needs to be computed by any mode solving technique. Consequently, also the investigated incident and reflected fields are regarded as a superposition of eigenmodes in free space. In the following steps, we choose a plane waves basis, where every plane wave is written in Dirac-notation as $|\mathbf{P}_{\mathbf{k}_\perp}^\pm\rangle$. Here, the $\pm$ sign either denotes forward $(+)$ or backward $(-)$ propagating waves. These are the incident and the reflected fields, respectively. $\mathbf{k}_\perp$ stands for the unique transverse wave vector of the plane wave $\mathbf{k}_\perp = (k_x, k_y)^\top$.

The interface problem, describing the coupling of the investigated field to the modes supported by the aperture, requires continuity of all tangential field components at the aperture $\mathbf{E}_\perp^{\text{freespace}}(x,y,z=0) \overset{!}{=} \mathbf{E}_\perp^{\text{aperture}}(x,y,z=0)$ (analogous for the magnetic fields $\mathbf{H}_\perp$). This can be written as follows

$$\underbrace{\int_{\mathscr{R}^2} i_{\mathbf{k}_\perp} |\mathbf{P}_{\mathbf{k}_\perp}^+\rangle}_{\text{incident field}} + \underbrace{\int_{\mathscr{R}^2} r_{\mathbf{k}_\perp} |\mathbf{P}_{\mathbf{k}_\perp}^-\rangle}_{\text{reflected field}} = \underbrace{\sum\!\!\!\!\!\!\int t_m |\mathbf{T}_m^+\rangle}_{\text{excited aperture modes}} \quad , \tag{11}$$

where $\sum\!\!\!\!\!\int$ symbolizes the discrete sum of the finite number of bound modes together with the integration of the infinite number of radiation modes in the system.

Eq. (11) fundamentally describes any coupling problem between any two structures and their supported eigenmodes. Conveniently, Eq. (11) can be solved by exploiting the unique properties of the electromagnetic modes $|\psi\rangle$ that are governed by an unconjugated reciprocity [39, 49]. An inner product can be defined as

$$\langle \psi_m | \psi_n \rangle = \int_{\mathscr{R}^2} [\mathbf{e}_m \times \mathbf{h}_n - \mathbf{e}_n \times \mathbf{h}_m] \mathbf{n}_z \, dx\, dy \quad , \tag{12}$$

in between the supported eigenmodes of the structures, where $\mathbf{n}_z$ is the unity vector in the z-direction. The orthogonality relation for the electromagnetic modes $|\psi\rangle$ of the same eigenmodal system reads

$$\begin{aligned} \langle \psi_m^+ | \psi_n^- \rangle &= \alpha_m^2 \, \delta_{mn} \,, \qquad & \langle \psi_m^+ | \psi_n^+ \rangle &= 0 \,, \\ \langle \psi_m^- | \psi_n^+ \rangle &= -\alpha_m^2 \, \delta_{mn} \,, \qquad & \langle \psi_m^- | \psi_n^- \rangle &= 0 \,, \end{aligned}$$

with α_m being the normalization factor. Based on this inner product, Eq. (11) can be solved self-consistently requiring the explicit knowledge about the limited number of bound modes, but also on the unlimited number of unbound radiation modes. The inclusion of the infinitely extended radiation modes on a numerically truncated grid is unfeasible. Therefore, further truncations depending on the system to be investigated are required.

In the considered case of image formation in collection-mode aperture SNOMs, the neglection of the reflection in Eq. (11) is a reasonable assumption. This approximation can be considered as the first order perturbation theoretical approach to describe the system. This corresponds to the assumption of a passive probe that does not perturb the investigated field components. This assumption was mentioned in [7], Rotenberg and Kuipers, to be mostly valid in practical situations.

By neglecting the reflection in Eq. (11), the problem reduces to the expansion of the investigated field into the modes supported by the aperture. The explicit representation of the investigated field in the plane wave basis is no longer necessary and thus the incident fields $\mathbf{E}(x,y)$ and $\mathbf{H}(x,y)$ will be renamed in Dirac-notation as $|\,{}^{\mathbf{E}}_{\mathbf{H}}\,\rangle$. For the description of the image formation process, the interest lies in the excitation strengths of the two propagative fundamental modes in the aperture. These excitation strengths can be calculated by projecting the

#256987 Received 6 Jan 2016; revised 7 Feb 2016; accepted 8 Feb 2016; published 19 Feb 2016

modes of the aperture onto the investigated field $t_{1,2}(x,y) = \langle \mathbf{T}^-_{1,2} | \, {}^{\mathbf{E}}_{\mathbf{H}} \, \rangle$. A detected image is thus described using Eq. (10) by

$$\mathscr{I}(x,y) = \left| \int_{\mathscr{R}^2} [\mathbf{e}^-_1(\tilde{x}-x,\tilde{y}-y) \times \mathbf{H}(\tilde{x},\tilde{y}) - \mathbf{E}(\tilde{x},\tilde{y}) \times \mathbf{h}^-_1(\tilde{x}-x,\tilde{y}-y)] \, \mathbf{n}_z \, d\tilde{x} \, d\tilde{y} \right|^2 + \left| \int_{\mathscr{R}^2} [\mathbf{e}^-_2(\tilde{x}-x,\tilde{y}-y) \times \mathbf{H}(\tilde{x},\tilde{y}) - \mathbf{E}(\tilde{x},\tilde{y}) \times \mathbf{h}^-_2(\tilde{x}-x,\tilde{y}-y)] \, \mathbf{n}_z \, d\tilde{x} \, d\tilde{y} \right|^2, \quad (13)$$

where $\mathbf{E}(\tilde{x},\tilde{y})$ and $\mathbf{H}(\tilde{x},\tilde{y})$ are the investigated field components at the position of the tip and $\mathbf{e}^-_{1,2}(\tilde{x},\tilde{y})$ and $\mathbf{h}^-_{1,2}(\tilde{x},\tilde{y})$ are the mode profiles of the two associated backward propagating mainly x- and y- polarized modes in the aperture and $(x,y)^T$ defines the position of the tip. This result is in close analogy to the more general results presented by Porto *et al.* in [9]. To be precise, within this early theory two scenarios fulfilling the requirements of reciprocity are evaluated. Then, on the one hand, a SNOM setup without the presence of the sample is considered in illumination mode. On the other hand, assuming a passive probe, the fields above the sample are considered in the second scenario. Expressions from these pioneering works are recovered if the eigenmodal-fields considered here are substituted with the reciprocal fields obtained by evaluating the SNOM-setup in illumination mode. In other words, we identify the eigenmodes supported by the aperture of the SNOM-setup as the source of illumination operating a SNOM-setup in illumination mode. Due to the deep subwavelength size of the aperture, only two eigenmodes are supported, which guarantees the agreement between both approaches [37, 38]. This identification can simplify the discussion of the image formation process in aperture based scanning near field optical microscopy as outlined in Sec. 2.

Acknowledgment

S.S. would like to thank Norik Janunts, Bayarjargal Narantsatsralt for helpful discussions and experimental measurements and David Musick for proofreading the manuscript. Support by the German Federal Ministry of Education and Research (KoSimO, PhoNa) and by the Thuringian State Government (MeMa) is acknowledged. We gratefully acknowledge partial financial support by the Deutsche Forschungsgemeinschaft (DFG) through CRC 1173 and Open Access Publishing Fund of Karlsruhe Institute of Technology.